Electrochemical Measurement of Effective Diffusivity in Hall-Heroult Electrolyte

Forced-convection mass transfer at the metal/bath interface during aluminum reduction from cryolitic melts was studied under reproducible convective conditions. A film of molten aluminum on a rotating molybdenum cylinder was the cathode. Concentration overpotential measured as a function of rotation rate, current density, and bath composition was converted to concentration differences between the bulk and the metal surface. Chosen as the basis for calculation of a mass transfer coefficient was the concentration of aluminum fluoride given by:

$$C_{AlF_3} = \frac{2\rho(100 - Al_2O_3\% - CaF_2\% - IMP\%)}{100M_{AlF_3}(CR + 2)}$$

where the amounts of indicated compounds are in weight percent, *IMP* designates impurities, *M* is molecular weight, ρ is the density of the melt, and *CR* is the cryolite ratio, the ratio of moles NaF to moles AlF_3. Agreement with a correlation for mass transfer to a rotating cylinder allowed the calculation of effective diffusivities for aluminum fluoride species, in alumina-saturated melts, of: $11.1 \pm 1.1 \times 10^{-5}$ cm^2/s at 1.8 *CR*; $11.4 \pm 1.7 \times 10^{-5}$ cm^2/s at 2.3 *CR*; $5.4 \pm 0.8 \times 10^{-5}$ cm^2/s at 3.0 *CR*; and $4.4 \pm 0.9 \times 10^{-5}$ cm^2/s at 4.0 *CR*.

John W. Burgman
Paul J. Sides
Department of Chemical Engineering
Carnegie Mellon University
Pittsburgh, PA 15213

Introduction

A mass transfer boundary layer exists at the metal/bath interface when aluminum is reduced from a cryolitic bath to form the metal. The major species in the melt are Na^+, AlF_6^{3-}, AlF_4^-, F^-, $Al_2O_2F_4^{2-}$, and $Al_2OF_6^{2-}$. Haupin and Frank (1981) reviewed the electrochemistry Hall/Heroult melts and concluded that the most probable cathode reactions are:

$$AlF_4^- + 3e^- \rightarrow Al + 4F^- \quad (1)$$

and

$$AlF_6^{3-} + 3e^- \rightarrow Al + 6F^- \quad (2)$$

with the aluminum fluoride species related through the rapid equilibrium

$$AlF_6^{3-} = AlF_4^- + 2F^- \quad (3)$$

that shifts to the left as the cryolite ratio, *CR*, increases. (The cryolite ratio is the ratio of the moles of sodium fluoride to the moles of aluminum fluoride.) In industrial melts having a *CR* of about 2, the fractions of AlF_4^- and AlF_6^{3-} are nearly equal; in melts of $CR > 4$, however, the fraction of AlF_4^- is negligible (Sterten, 1980). Haupin and Frank (1981) also concluded that the following reactions are reasonable mechanisms by which aluminum fluorides are complexed into oxyfluoroaluminates in the presence of alumina:

$$4AlF_6^{3-} + Al_2O_3 \rightarrow 3Al_2OF_6^{2-} + 6F^- \quad (4)$$

and

$$AlF_6^{3-} + Al_2O_3 \rightarrow \frac{3}{2}Al_2O_2F_4^{2-} \quad (5)$$

Reaction 4 predominates at low alumina concentration and reaction 5 predominates at high alumina concentration. Thus the melt consists primarily of four types of species: sodium ions,

Correspondence concerning this paper should be addressed to P. J. Sides.

fluoride ions, oxyfluoroaluminate ions, and aluminum fluoride ions. Impurities or additives such as calcium ion are also present.

The behavior of these species in the boundary layer near the cathode is complex. The aluminum fluoride anions migrate away from the cathode but diffuse toward it with a net flux to the cathode where the aluminum is reduced and fluoride ion is released. The concentration of sodium ion at the metal surface increases over the bulk value so that diffusion away from the cathode balances migration toward it. Oxyfluoroaluminate anions are probably not reduced directly; consequently, their flux at the surface is zero. Electroneutrality is satisfied throughout the boundary layer. The net effect is an increase in the *CR* at the metal/bath interface over the value in the bulk. The ionic concentration gradients are a function of the cell hydrodynamics, transport properties, and the current density.

Although mass transport in the cathode boundary layer ordinarily does not limit the rate of aluminum deposition, the increase in the *CR* at the metal/bath interface affects cell operations in several ways. At industrial current densities, the composition differences across the boundary layer engender a concentration overpotential of about 100 mV (Haupin and Frank, 1981; Thonstad and Rolseth, 1978a) A high *CR* at the metal/bath interface, furthermore, promotes the dissolution of reduced species into the electrolyte where reoxidation by CO_2 near the anode decreases the cell current efficiency (Arthur, 1974; Haupin, 1960; Thonstad, 1965; Yoshida and Dewing, 1972b). Electrolyte can precipitate on the cathode due to increases in the *CR* at the metal/bath interface (Thonstad, 1978b). The increased Na^+ content of the electrolyte adjacent to the aluminum pad increases sodium content of the metal product and the carbon cell lining, which is particularly important in modern cells operating with fewer disturbances. The mass transfer at the cathode also can determine the lifetime of an inert anode.

The consequences of the increased *CR* at the metal/bath interface are well known, but the mass transfer phenomena responsible have not been quantified satisfactorily. Del Campo et al. (1981) proposed a model that allowed for the dissociation of aluminum trifluoride, but the division of the mass transfer boundary layer into sharp regions where dissociation of the complex ions occurs seems no less arbitrary than definition of an overall mass transfer coefficient. Diffusion measurements in cryolitic melts have been limited. Harari et al. (1970) found the self diffusion coefficient for Al to be 6.9×10^{-5} cm^2/s in 3.0 *CR* bath at 1,051°C and 7.4×10^{-5} cm^2/s in 6.4 *CR* bath at 1,034°C. Lantelme and Chemla (1968) reported a diffusivity of 1.8×10^{-5} cm^2/s for AlF_6^{3-} in cryolite at 1,050°C. Previous workers have measured concentration overpotential as a function of nonuniform current densities and irreproducible convective conditions (Thonstad and Rolseth, 1978a; Thonstad and Rolseth, 1978b; Borisoglebskii et al., 1971; Lozhkin and Popov, 1968). Del Campo et al. (1981) used a rotating disk that has reproducible flow characteristics, but the disk geometry must have a complicated nonuniform ternary current distribution that makes simple application of the Levich equation questionable. Furthermore, the flatness of the disk must have been compromised to some extent by the deposition of aluminum.

In this work we present the effect of bath chemistry, bath motion, and current density on cathodic overpotential measured under the reproducible convective conditions and uniform current density of a rotating cylinder electrode. Agreement with an established correlation for mass transfer to a rotating cylinder allowed the calculation of effective diffusivities for aluminum fluoride species, in alumina-saturated melts, of: $11.1 \pm 1.1 \times 10^{-5}$ cm^2/s at 1.8 *CR*; $11.4 \pm 1.7 \times 10^{-5}$ cm^2/s at 2.3 *CR*; $5.4 \pm 0.8 \times 10^{-5}$ cm^2/s at 3.0 *CR*; and $4.4 \pm 0.9 \times 10^{-5}$ cm^2/s at 4.0 *CR*.

Experimental

Cell design

The experimental cell design for measuring cathodic overpotential under reproducible convective conditions appears in Figure 1. [Discussed elsewhere is a similar cell design for determining an effective diffusivity of the aluminum-bearing species (Burgman and Sides, 1987). A viscous deposit on the cathode, however, interfered with the experiments. After further study, the cell described here was designed to eliminate formation of the troublesome deposit caused by boron nitride components. The deposit is described in more detail in the Appendix.] The graphite crucible, with a 0.6 cm diameter nickel 200 lead connection (not shown), was the counter electrode. An alumina separator prevented aluminum reoxidation by the anodic products by impeding mass transfer between the anode and cathode compartments. Molten cryolite in the pores of the alumina maintained ionic conductivity between the compartments. The concentric cylinder design consisting of the graphite crucible, the alumina separator, and the rotating cylinder electrode ensured a uniform current distribution on the wetted cathode surface. The alumina bottom plates, which were stable in the melt because it was saturated with alumina, insulated the bottom of the crucible. The graphite cell cover minimized the change in electrolyte composition because of vaporization of sodium aluminum fluorides from the bath. Both the alumina separator and an Ar or N_2 purge were eliminated when overpotential measurements were found to be the same without them.

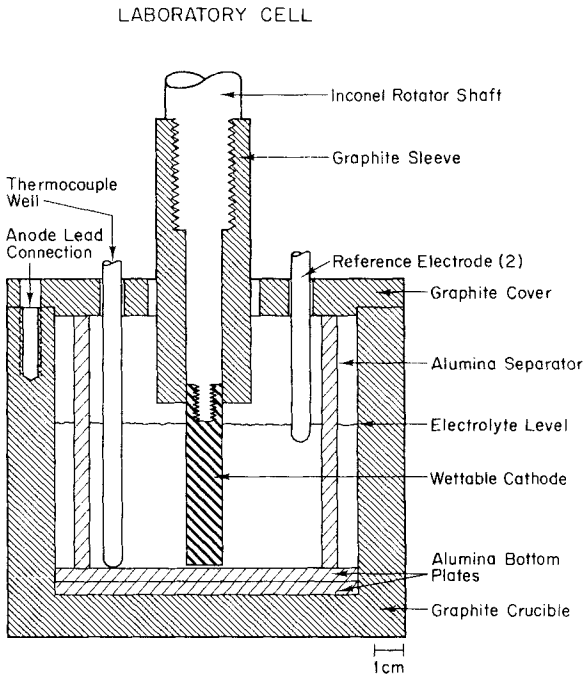

Figure 1. Experimental cell.

Two wetted molybdenum hook (MWH) reference electrodes (Burgman et al., 1986) and an Inconel-sheathed chromel-alumel thermocouple housed in a 0.48 cm ID closed one end alumina tube were also present in the cell. The reference electrodes did not rest on the bottom of the cell, but were elevated nearly out of the current lines of the cell because other experiments showed that the reference electrodes could be polarized away from their rest potential when placed in an electric field.

The electrodes shown in Figure 1 were 0.32-, 0.64-, and 1.27-cm-diameter molybdenum cylinders fastened to an electronically conducting Inconel 601 shaft extending through a graphite sleeve that protected the shaft from attack by cryolite. The electrolyte level in the cell, maintained at 5.1 cm, defined the active length of the rotating cylinder electrode. Positioning the cathode just above the bottom plate, Figure 1, geometrically limited the current reaching the bottom of the cathode, ensuring that the sides were most electrochemically active. The 90° angle between the molybdenum cathode and both the alumina bottom plate and the electrolyte surface guaranteed a nearly uniform current distribution on the cathode. A Pine Instruments Analytical Rotator, Model ASR2 rotated the electrode. The eccentricity of the rotating cylinders was 0.007 ± 0.005 cm. The formation of a vortex in the electrolyte was not observed at the relatively low rotation rates (less than 600 rpm) of this experiment.

An aluminum-coated-molybdenum cathode was examined with a scanning electron microscope. The cathode, used in several experiments, was sectioned, mounted, and polished. The scanning electron micrograph and elemental maps of molybdenum and aluminum appear in Figure 2. A 75- to 100-μm-thick, aluminum-rich outer layer, containing a small percentage of molybdenum, covered the molybdenum substrate verifying that the experimental cathode consisted of an aluminum/molybdenum alloy coating molybdenum. The distinct boundary between the two uniform layers indicated that molybdenum and aluminum did not significantly interdiffuse. The alloy probably contained the 3% saturation concentration of molybdenum in aluminum (Thonstad and Rolseth, 1978a).

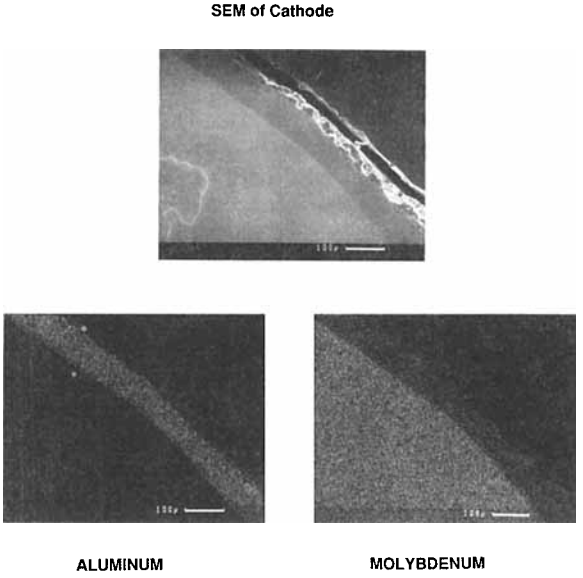

Figure 2. Scanning electron micrograph of a cathode cross section with elemental maps of aluminum and molybdenum.

The experimental cell sat in a 15-cm-ID, 18-cm-deep Inconel 601 containment vessel purged with 5 L/min nitrogen that flowed from bottom to top to eliminate oxygen entrainment (Burgman, 1986). The 1.5 cm gap between the graphite crucible and the Inconel container contained 6–8 mesh carbon pellets to inhibit oxidation of the crucible by preferentially burning and by limiting convective air currents. A Thermcraft, 4.6-kW, 20-amp, single-temperature-zone furnace controlled by a Barber Colman 560 Series microprocessor heated the cell and containment vessel.

Chemicals

Natural Greenland cryolite, Pt. Comfort AlF_3, metal grade Al_2O_3, and Alfa Products ACS Grade NaF were used in this study. The experimental cell contained one of four bath mixtures summarized in Table 1. The alumina concentration cited in Table 1 corresponds to saturation at 1,000°C. CaF_2 was present in the experimental melts because it was found in the cryolite and AlF_3 used in the mixtures and is found in industrial cells. The WMH reference electrodes contained a bath mixture identical to that used in the cell and minimum 99.99% pure aluminum. The Alfa Products molybdenum lead wires and cathodes were 99.97% pure.

Measurement system

The electrochemical measurement system appears in Figure 3. A Hewlett/Packard 3497A data acquisition/control unit (not shown) controlled a Hewlett/Packard 6269B DC power supply. A solid state switch, International Rectifier IRF252, interrupted the current in the counter electrode circuit with a delay of 125 nanoseconds. Voltage pulses with rise and fall times of less than 15 ns from an Interstate Electronics Corporation function generator model F77/R toggled the switch. The potential difference between the working electrode and the reference electrode appeared on a Nicolet Explorer I digital storage oscilloscope. The function generator simultaneously opened the switch, which eliminated the included ohmic voltage, and triggered the oscilloscope to monitor the potential difference.

Open circuit potential

Accurate measurement of overpotential required knowledge of the open circuit working electrode potential. Because the open circuit potential varied slowly during the experiment, we period-

Table 1. Electrolyte Composition and Properties

CR	1.8	2.3	3.0	4.0	Reference
NaF (wt. %)	42.9	46.7	51.5	57.0	
AlF_3 (wt. %)	47.6	40.6	34.3	28.5	
Al_2O_3 (wt. %)	8.2	10.6	12.8	13.3	Foster, 1964 Foster, 1975
CaF_2 (wt. %)	0.4	1.2	0.7	0.7	
impurities (wt. %)	0.9	0.9	0.7	0.6	
μ (cp)	2.1	2.9	3.7	4.3	Grjotheim *et al.*, 1977
ρ (g/cm^3)	1.96	2.00	2.04	2.07	Grjotheim *et al.*, 1977

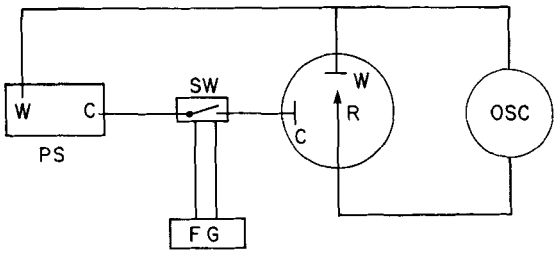

Figure 3. Electrochemical measurement system.
R = reference
W = working
C = counter
PS = DC power supply
SW = interruption switch
FG = function generator
OSC = oscilloscope

ically opened the circuit and measured the potential between the reference and working electrode; within 10 to 30 s after current was halted, stable baseline potentials were achieved. The reference electrode itself was checked periodically by measuring the potential of an aluminum-coated-wire (ACW), placed in the electrolyte, with respect to the WMH reference electrode. The aluminum-coated-wire reference electrode consisted of an alumina-sheathed, 0.1-cm-diameter molybdenum wire placed, for 5 minutes, into an aluminum pool at 825°C. The potential between an ACW reference electrode and the WMH reference electrode was monitored continuously for about 1 minute on a Nicolet Explorer I Oscilloscope, after which the ACW reference electrode became continually more positive as the aluminum activity on the molybdenum wire decreased. The ACW was adjusted 5 mV for the thermoelectric potential, at 1,000°C, of molybdenum with respect to Inconel. The reproducibility of the ACW check was approximately 3 mV.

Procedure

Current densities were 200, 400 and 600 mA/cm^2. Rotation of 0.32-, 0.64-, and 1.27-cm-diameter molybdenum cylinders, from 100 to 500 rpm, gave Reynolds numbers from 40 to 3,800 and produced turbulent flow for each cathode and rotation rate (Schlichting, 1979). To begin an experiment, an electrode was lowered into the cell and allowed to come to temperature, 1,000°C. A current density of 200 mA/cm^2 was applied for 3 to 5 minutes to deposit aluminum on the molybdenum substrate, after which the open circuit baseline potential measurement between the cathode and the reference electrode was checked. If this baseline value was within several millivolts of null, the cathode was behaving as an aluminum electrode without mixed potentials due to impurities or a nonuniform coating. A typical trial began at 200 mA/cm^2 and consisted of three to five overpotential measurements at 100 rpm and followed by three to five more measurements at 150, 200, 300, 400 and 500 rpm. The rotation rate was returned from 500 to 100 rpm and the overpotential was measured several times to check for the reproducibility and fast response indicative of a uniform, aluminum surface. An open circuit baseline potential between the cathode and the WMH reference electrode was then determined and compared to the initial baseline measurement. If the values were within 5 mV, the procedure was repeated with current densities of 400 and 600 mA/cm^2.

Results

The raw experimental data consisted of overpotentials measured as a function of rotation rate for each *CR* in alumina-saturated bath. Overpotentials decreased with increasing rotation rate, indicative of the role of mass transfer in the process, for each set of conditions. The overpotentials approached zero at high rotation rates, because the surface overpotential is negligibly small for this system (Thonstad, 1978a; Piontelli, 1956; Piontelli, 1963), and increased, as expected, with current density for a given cathode diameter and rotation rate. At constant current and rotation rate, overpotential decreased with increasing cathode diameter. Data was obtained for 1.8, 2.3, 3.0 and 4.0 *CR* alumina-saturated baths. The raw data can be found in Burgman's thesis (1988).

Discussion

Discussion of the results of these experiments is divided into three parts. We first define a mass transfer coefficient of aluminum-bearing species to the electrode surface and, second, demonstrate that the mass transfer coefficient can be correlated with Eisenberg et al.'s (1954) equation for the rotating cylinder. Implicit in the latter part is the determination of an effective diffusivity of the aluminum-bearing species. The third part is a discussion of why mass transfer to an electrode consisting of a thin liquid film in such a geometry obeys a correlation determined for a solid electrode.

Definition of a mass transfer coefficient

The overpotential data were analyzed in terms of the mass transfer coefficient, k, defined by the following equation:

$$\frac{i}{nF} = k(C_{j,b} - C_{j,s}) \tag{6}$$

where i is the current density, k is the mass transfer coefficient, and $C_{j,b}$ and $C_{j,s}$ are the concentrations of species j in the bulk electrolyte and at the cathode surface, respectively. For this reaction, aluminum reduction, n is three equivalents per mole.

The species j on which to base the concentration for the calculation of mass transfer coefficient, k, should bear aluminum to the electrode and have a well-defined concentration. The concentration of aluminum trifluoride accounts for both of the aluminum fluoride complex anions, coupled by equilibrium reaction (Eq. 3), that are consumed at the electrode; the trivalent of these two anions, however, complexes with the oxyfluoroaluminates according to reactions 4 and 5, which complicates the choice for species j. In view of this complexity, we reduced the data according to four aluminum fluoride concentration models, each expressing the influence of Al_2O_3 differently. In each of the four models, the concentration of AlF_3 is given by

$$C_{AlF_3} = \frac{2\rho(100 - Al_2O_3\% - CaF_2\% - IMP\%)}{100M_{AlF_3}(CR + 2)} \tag{7}$$

where M_{AlF_3} is the molecular weight, ρ is the density of the melt, $Al_2O_3\%$ is the weight percent of Al_2O_3, $CaF_2\%$ is the weight percent of CaF_2, and $IMP\%$ is the weight percent of impurities. The

concentration of alumina is given by

$$C_{Al_2O_3} = \frac{\rho Al_2O_3\%}{100 M_{Al_2O_3}} \tag{8}$$

where $M_{Al_2O_3}$ is the molecular weight. The concentration of alumina at the surface corresponds to the saturation concentration for the *CR* at the surface.

In Model 1, C_j is the total concentration of AlF_3.

$$C_j = C_{AlF_3} \tag{9}$$

Model 1 ignores complexing of AlF_6^{3-} with Al_2O_3. In Model 2, C_j is the concentration of aluminum trifluoride minus the amount of AlF_6^{3-} complexed with Al_2O_3.

$$C_j = C_{AlF_3} - C_{Al_2O_3} \tag{10}$$

Model 3 represents C_j as the total concentration of aluminum-bearing complexes.

$$C_j = C_{AlF_3} + \frac{1}{2} C_{Al_2O_3} \tag{11}$$

In Model 4, C_j is the total concentration of trivalent aluminum.

$$C_j = C_{AlF_3} + 2C_{Al_2O_3} \tag{12}$$

Note that Models 2, 3, and 4 refer to the equilibrium between aluminum fluoride anions and alumina as expressed by Eq. 5.

To calculate the mass transfer coefficients, the bulk concentration was calculated directly from the bulk *CR* and the surface concentration was determined by comparing the measured concentration overpotential with data for the EMF of the aluminum electrode as a function of the *CR* (Thonstad, 1978b; Yoshida, 1972a), that is, the surface *CR* was the composition corresponding to a change in EMF equal to the overpotential. The concentration difference between the surface and the bulk, combined with the current, n, and F according to Eq. 6, determined the mass transfer coefficient. We processed the data through all of the models and the results for the effective diffusivities based on these models are presented and discussed.

Comparison of the results of the correlation

We compared the mass transfer coefficients at a given current density, bath composition, and rotation rate to the general mass transfer correlation for a rotating cylinder of Eisenberg, et al. (1954).

$$\frac{kd}{D} = 0.0791 \left(\frac{Vd}{\nu}\right)^{0.70} \left(\frac{\nu}{D}\right)^{0.356} \tag{13}$$

where

kd/D = Sherwood number, Sh
Vd/ν = Reynoldes number, Re
ν/D = Schmidt number, Sc
k = mass transfer coefficient, cm/s
d = diameter of molybdenum cylinder, cm
D = diffusion coefficient, cm^2/s
V = tangential velocity of molybdenum cylinder, cm/s
ν = kinematic viscosity, cm^2/s.

The Reynolds number was based on the film density and film viscosity, defined as the arithmetic mean between the surface and bulk values. The Sh and Sc numbers were calculated for each point with the single effective diffusivity that optimizes the agreement of the group of data with the correlation (Eq. 13) for a particular bulk composition. The dependence of $Sh/Sc^{0.356}$ on Re for the 1.8 *CR* bath appears in Figure 4 with concentration Model 1 as the basis. The straight line in the figure is the correlation having a slope of 0.7. Figure 4 demonstrates that the mass transfer in this case is well described by the correlation. The filled points near a Reynolds number of 50 are for data obtained with the 0.32-cm-diameter cathode rotating at 100 rpm. These data were not included in the statistical analysis to determine the effective diffusivity because a positive deviation of this data from the correlation was common to each electrolyte composition. The measured overpotentials were lower than expected, possibly indicating that free convection was stronger than forced convection at these conditions. The filled points at Reynolds numbers above 800 were also excluded from the statistical analysis because the measured overpotentials at the highest Reynolds numbers were often less than 10 mV and the reproducibility of the measurements was about 5 mV, which gave large errors in this range. Similar plots for 2.3, 3.0, and 4.0 *CR* baths appear in Burgman's thesis (1988).

The diffusion coefficient, D, is the only unknown in correlation (Eq. 13), and is determined implicitly by optimizing the position of the data as a group with respect to the correlation. It is an "effective diffusivity" because it represents an average across the mass transfer boundary layer. The average reflects

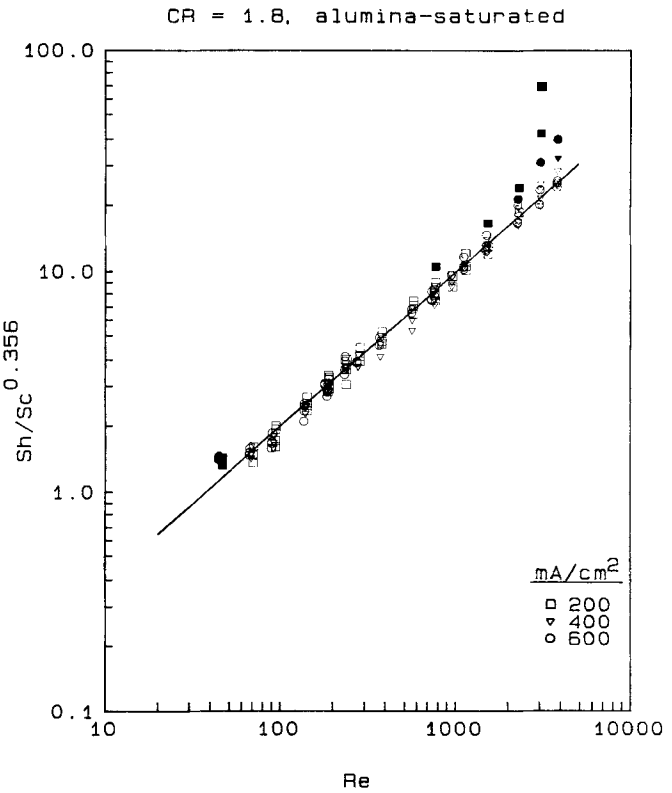

Figure 4. Dimensionless mass transfer coefficient as a function of Reynolds number.
At 200, 400 and 600 mA/cm² in 1.8 *CR*, alumina-saturated bath: filled points are excluded from the statistical analysis.

the concentration model employed, the influence of transference, the nonzero interfacial velocity, as well as variations in electrolyte properties due to changes in composition. The effective diffusivities, determined for each bath composition and with each concentration model, appear in Table 2.

Use of Model 1, the AlF_3 concentration, as the basis of the mass transfer driving force, yielded results that agreed with the correlation for all bath compositions tested; it is the basis of Figure 4. A plot of effective diffusivity as a function of *CR*, determined using Model 1, appears in Figure 5. Comparable values of 1.8 and 2.3 *CR* baths are followed by a decrease in effective diffusivity with increasing *CR*. The effective diffusivities exhibit the general behavior of decreasing the increasing viscosity as also shown in Figure 5 in which the diffusivity and reciprocal viscosity are plotted versus the *CR*.

The three other concentration models yielded less satisfactory results. Model 2, consideration of complexing of Al_2O_3 with AlF_6^{3-}, gave erratic values for the effective diffusivity and a twofold increase in the residual sum of squares at the highest *CR*. Measured effective diffusivities ranged from 5.2×10^{-5} to 38.7×10^{-5} cm^2/s according to this concentration model. Since the EMF of an aluminum electrode becomes a weaker function of *CR* as *CR* increases, high overpotentials in the 4.0 *CR* bath correspond to large increases in *CR* and related decreases in alumina content across the mass transfer boundary layer; these effects coupled with Model 2 produce large mass transfer coefficients. For example, with a 0.32 cm diameter cathode, rotating at 200 rpm, an overpotential of -63.4 mV was measured at 600 mA/cm^2, which corresponds to a 6.25 *CR*, 7.3 wt. % alumina bath composition at the surface of the electrode. The concentration of aluminum fluorides in the bulk and at the surface is 4.35 and 3.95 mmol/cm^3, respectively, for Model 2, compared to 7.02 and 5.44 mmol/cm^3 for Model 1. The consideration of complexing with alumina reduces the bulk aluminum fluoride concentration 80% more than it reduces the surface concentration, which produces a mass transfer coefficient of 5.3×10^{-3} cm/s and an effective diffusivity of 28.0×10^{-5} cm^2/s. Model 3, the total concentration of aluminum-bearing complexes, yielded values at a *CR* of 4.0 that were not as precise as given by Model 1. The use of total Al^{3+}, Model 4, yielded an approximately 90% increase in the residual sum of the squares for the high ratio, because of the strong influence of alumina content that diminishes the contribution of aluminum fluoride concentration changes across the mass transfer boundary layer, as was found in the use of Model 2. In general, the greater the allowance for alumina in the concentration model, the less precise the results, which is evidence that oxyfluoroaluminates do not participate directly in the electrode reaction. If these complexes participated in the cathode reaction, allowance for alumina would improve the agreement at the highest *CR*. This evidence also agrees with the finding of Thonstad and Rolseth (1978b) that cathodic overvoltage does not depend on concentration of alumina. If alumina participated in the cathode reaction, some dependence would have been evident.

Table 2. Effective Diffusivities

	D_{eff}, $\times 10^5$ cm^2/s			
CR	Model 1	Model 2	Model 3	Model 4
1.8	11.1 ± 1.1	6.9 ± 0.7	15.2 ± 1.5	85. ± 8.6
2.3	11.4 ± 1.7	6.9 ± 1.0	15.8 ± 2.4	104 ± 17
3.0	5.4 ± 0.8	3.9 ± 0.7	6.6 ± 1.0	15.0 ± 3.5
4.0	4.4 ± 0.9	9.2 ± 7.2	3.4 ± 0.8	1.9 ± 0.6

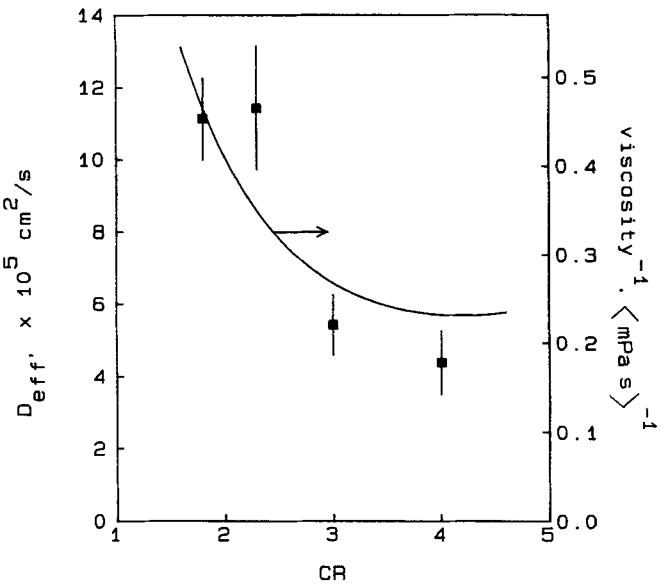

Figure 5. Effective diffusivity of aluminum fluoride species and reciprocal melt viscosity as a function of *CR* in alumina-saturated baths.

Applicability of the correlation of this case

Remaining is the question of why the mass transfer in this case, in which a relatively thin liquid film of aluminum coats a solid cylinder, agrees with a correlation developed for a solid rotating cylinder. The explanation is based on the rough equality of the kinematic viscosities of the two liquid phases, the high interfacial tension between the aluminum and the bath (approximately 500 dyne/cm) and the thinness of the aluminum film relative to the diameter of the cylinder. The kinematic viscosity of the aluminum is 30% higher than that of the electrolyte at the lowest *CR* and 30% lower than the kinematic viscosity of the electrolyte at the highest *CR*; hence, the film rotates slightly more with the cylinder than it is retarded by the bath at the low *CR* and *vice versa* at the highest *CR*. The high interfacial tension indicates that the aluminum bath interface is rigid to radial momentum transport, that is, there are no waves and no dimples due to the turbulent flow caused by the rotating cylinder. If the interface is rigid to radial motion, the electrolyte cannot distinguish between a liquid surface rotating *at the velocity of the electrolyte-aluminum interface* and a solid surface rotating at that velocity; hence, the mass transfer correlation derived for a solid cylinder describes the mass transfer in this case as long as the surface velocity and diameter of the cylinder used in the Reynolds number are the surface velocity and diameter of the *solid cylinder plus the film*. The consequence of the thinness of the film is that the velocity of the interface is ten to twenty percent smaller than the velocity of the solid cylinder in the worst case and the diameter of the solid cylinder plus the film is from one to six percent larger than the diameter of the solid cylinder. We have estimated the maximum error involved in basing the Reynolds number and diameter on the solid cylinder and found it to be the amount of the error we obtained in the experiment.

Acknowledgments

The authors gratefully acknowledge support for this work from the Aluminum Association and Electric Power Research Institute. The writers would like to thank Dr. Nolan Richards and Reynolds Aluminum for special assistance with chemical analysis.

Appendix: Boron Nitride and Formation of a Viscous Deposit

Aluminum did not form a uniform film during deposition in a design (Burgman, 1987) that used a boron nitride separator and bottom pieces. The aluminum was incorporated into a viscous deposit on the electrode that was black when cooled. The mass of the deposit was at least ten times greater than the mass of aluminum formed. An SEM-EDX analysis of the viscous deposit revealed no unusual impurity levels for elements of atomic number greater than 20. A complete elemental analysis showed the viscous deposit to consist principally of the cryolitic components, sodium, aluminum, and fluorine, and 1% boron that must have come from the boron nitride parts used in the cell (Richards, 1986). Samples of 2.3 *CR* catholyte contained between 0.03 and 0.18% boron (Richards, 1986). The dependence of formation of the deposit on boron was established with a simple experiment in which a molybdenum cathode, in a graphite crucible containing a 2.3 *CR*, 1.3% Al_2O_3, 1.3% CaF_2, boron-free electrolyte, was polarized at 0.4 A/cm^2 to form an aluminum film free of viscous deposit.

Because there was more boron in the viscous deposit than in the bulk electrolyte, it must have accumulated through the reduction of B_2O_3 present in the BN cell components. (Union Carbide Grade HBC BN contains a maximum of 1% oxygen.) The mechanism is feasible because B_2O_3 has an unlimited solubility in cryolite and boron is more noble than aluminum (Grjotheim et al., 1977). At 1,000°C, the solubility of boron in aluminum is 0.25 wt. %, larger fractions of boron in aluminum result in the formation of solid AlB_{12} (Mondolfo, 1976; Van Horn, 1967).

An order of magnitude calculation, based on the current passed and the mass of viscous deposit formed, indicated that the deposit consisted of 90% electrolyte and 10% reduced species, of which boron contributed 1%. Therefore, the reduced fraction contained principally liquid Al (with 0.25% dissolved B) and a smaller amount of solid AlB_{12}. The fact that molten aluminum was not visually detected in the deposit can be explained if solid AlB_{12} on the surface of Al droplets prevented coalescence, creating a highly viscous dispersion of droplets in electrolyte. The black color of the deposit after cooling was consistent with the observation that solidified mixtures of dispersed aluminum droplets ranging in size from 3 to 300 μm in cryolite are black near the surface of the particles (Grjotheim et al., 1977).

Notation

C = concentration of species, mol/cm^3
CR = cryolite ratios, moles NaF/mol AlF_3
d = diameter of the rotating cylinder, cm
D = effective diffusivity of aluminum bearing species, cm^2/s
k = mass transfer coefficient, cm/s
V = tangential velocity of the rotating cylinder surface, cm/s

Greek letters

ν = kinematic viscosity, cm^2/s

Subscripts

j = species j
b = bulk electrolyte
s = cathode surface

Literature Cited

Arthur, A. M., "The Solubility of Aluminum in Cryolite-Alumina Melts and the Mechanism of Metal Loss," *Met. Trans.*, **5,** 1225 (1974).

Borisoglebski, Y. V., M. M. Vetyukov, and V. B. Vinokurov, "An Examination of the Cathodic Overvoltage when Electrolyzing Aluminum in Cryolite-Alumina Melts," *Sov. J. Non-Ferrous Met.*, **12,** 42 (1971).

Burgman, J. W., "Mass Transfer at the Metal/Bath Interface in Hall/Heroult Electrolysis," PhD Thesis, Carnegie Mellon Univ. (Mar., 1988).

Burgman, J., J. Leistra, and P. Sides, "Aluminum/Cryolite Reference Electrodes for Use in Cryolite-Based Melts," *J. Electrochem. Soc.*, **133,** 496 (1986).

Burgman, J., and P. Sides, "Mass Transfer at the Hall Cell Cathode," *Light Met.*, 233 (1987).

Del Campo, J., J. Millet, and M. Rolin, "L'Electrolyse de l'Alumine dans la Cryolithe Fondue: Etude du Mechanisme de Decharge Cathodique a l'Aide de l'Electrode a Disque Tournant," *Electrochim. Acta,* **26,** 59 (1981).

Eisenberg, M., C. W. Tobias, and C. R. Wilke, "Ionic Mass Transfer and Concentration Polarization at Rotating Electrodes," *J. Electrochem. Soc.*, **101,** 306 (1954).

Grjotheim, K., C. Krohn, M. Malinovsky, K. Matiasovsky, and J. Thonstad, "Aluminum Electrolysis: The Chemistry of the Hall-Heroult Process," Aluminum-Verlag, Dusseldorf (1977).

Harari, D., F. Lantelme, and M. Chemla, "Mesure des Coefficients de Diffusion de Al dans les Bains de Flourures de Sodium et d'Aluminium," *C. R. Acad. Sc. Paris,* **C270,** 653 (1970).

Haupin, W. E., "Metal Mists and Aluminum Losses in the Hall Process, *J. Electrochem. Soc.*, **102,** 232 (1960).

Haupin, W. E., and W. B. Frank, "Electrometallurgy of Aluminum," *Comprehensive Treatise of Electrochemistry,* Bockris et al., eds., 301 (1981).

Lantelme, F., and M. Chemla, "Study of the Diffusion of Sodium and Fluorine Ions in Fused Cryolite," *Compt. Rend. Acad. Sc. Paris,* **C267,** 281 (1968).

Lozhkin, L. N., and A. P. Popov, "Some Characteristics of the Cathode Process in Electrolysis of Cryolite-Alumina Melts," *J. Appl. Chem. USSR,* **41,** 2277 (1968).

Mondolfo, L. F., *Aluminum Alloys: Structure and Properties,* Butterworth, London (1976).

Piontelli, R., "Discussion: Sodium-Aluminum Equilibria in Cryolite-Alumina Melts," *J. Electrochem. Soc.*, **103,** 705 (1956).

Piontelli, R., "Polarization Phenomena in Aluminum Cells," *Proc. Conf. on Electrochem.*, 932 (1963).

Richards, N., Personal communication, Reynolds Metals Co.'s Reduction Laboratory (1986).

Schlichting, H., *Boundary-Layer Theory,* McGraw-Hill, New York (1979).

Sterten, A., "Structural Entities in NaF-AlF Melts Containing Alumina," *Electrochim. Acta,* **25,** 1673 (1980).

Thonstad, J., "The Solubility of Aluminum in NaF-AlF-Al O Melts," *Can. J. Chem.*, **43,** 3429 (1965).

Thonstad, J., and S. Rolseth, "On the Cathodic Overvoltage on Aluminum in Cryolite-Alumina Melts: I," *Electrochim. Acta,* **23,** 223 (1978a).

Thonstad, J., and S. Rolseth, "On the Cathodic Overvoltage on Aluminum in NaF-AlF-Al O Melts: II," *Electrochim. Acta,* **23,** 233 (1978b).

Van Horn, K. R., ed., *Aluminum: 1. Properties, Physical Metallurgy and Phase Diagrams,* Amer. Soc. for Metals, Metals Park, OH (1967).

Yoshida, K., and E. W. Dewing, "Activities in NaF-AlF Melts Saturated with Al_2O_3," *Met. Trans.*, **3,** 683 (1972a).

Yoshida, K., and E. W. Dewing, "The Apparent Solubility of Aluminum in Cryolite Melts," *Met. Trans.*, **3,** 1817 (1972b).

Manuscript received Nov. 30, 1987, and revision received May 10, 1988.